

Two-Real-Singlet-Model Benchmark Planes

Tania Robens 

Division of Theoretical Physics, Ruder Boskovic Institute, 10002 Zagreb, Croatia; trobens@irb.hr

Abstract: In this manuscript, I briefly review the Benchmark Planes in the Two-Real-Singlet Model (TRSM), a model that enhances the Standard Model (SM) scalar sector by two real singlets that obey a $\mathbb{Z}_2 \otimes \mathbb{Z}'_2$ symmetry. In this model, all fields acquire a vacuum expectation value, such that the model contains in total three CP-even neutral scalars that can interact with each other. All interactions with SM-like particles are inherited from the SM-like doublet via mixing. I remind the readers of the previously proposed benchmark planes and briefly discuss possible production at future Higgs factories, as well as regions in a more generic scan of the model. For these, I also discuss the use of the W-boson mass as a precision observable to determine allowed/excluded regions in the models' parameter space. This work is an extension of a white paper submitted to the Snowmass process.

Keywords: collider phenomenology; extended scalar sectors; LHC; Higgs factories

1. Introduction and Model

After the discovery of a scalar boson that complies very well with the predictions for the Standard Model (SM) Higgs sector (see e.g., [1,2] for recent experimental summaries), particle physics has entered an exciting era. One crucial question is whether the scalar we are observing indeed corresponds to the Higgs boson predicted by the SM or whether it is part of an extended scalar sector, introducing additional scalar states. For many years, many models have been suggested that extend the SM scalar sector by additional electroweak singlets, doublets, or other multiplets.

From a bottom up approach, the easiest extension of the SM scalar sector is the extension by an additional gauge singlet, where further symmetries can be imposed in order to reduce the number of free parameters in the model. Such extensions have been, e.g., discussed in [3–5], with a more recent update on the allowed parameter space in [6]. Such models can also allow for a strong first-order electroweak phase transitions; see, e.g., the discussion in [7,8] and references therein. A discussion of such models without an additional symmetry can, e.g., be found in [9,10]

The simple singlet extensions only allow for one additional scalar. Experimental searches, however, now start to investigate so called non-symmetric production modes of the form

$$p p \rightarrow h_a \rightarrow h_b h_c,$$

where $h_{a,b,c}$ here denote scalar states with different masses; first results for such searches have been presented in [11,12]. To allow for such final states, at least one additional scalar needs to be among the particle content of the considered model. Although many new physics extensions allow for such scenarios, again the most straightforward realization is a model where one additional scalar field is added that transforms as a singlet under the SM gauge group. This is the model that this work focusses on.

The model discussed here has been proposed in [13], and I refer the reader to that reference for a detailed discussion of model setup and constraints. I briefly repeat the generic features for completeness. The work presented here is an extension of a Snowmass white paper [14]. Similar models have, e.g., been discussed in [15–27].

The potential in the scalar sector is given by



Citation: Robens, T.

Two-Real-Singlet-Model Benchmark Planes. *Symmetry* **2023**, *15*, 27.<https://doi.org/10.3390/sym15010027>

Academic Editor: Dubravko Klabučar

Received: 15 October 2022

Revised: 7 December 2022

Accepted: 15 December 2022

Published: 22 December 2022



Copyright: © 2022 by the authors. Licensee MDPI, Basel, Switzerland. This article is an open access article distributed under the terms and conditions of the Creative Commons Attribution (CC BY) license (<https://creativecommons.org/licenses/by/4.0/>).

$$V(\Phi, S, X) = \mu_\Phi^2 \Phi^\dagger \Phi + \lambda_\Phi (\Phi^\dagger \Phi)^2 + \mu_S^2 S^2 + \lambda_S S^4 + \mu_X^2 X^2 + \lambda_X X^4 \\ + \lambda_{\Phi S} \Phi^\dagger \Phi S^2 + \lambda_{\Phi X} \Phi^\dagger \Phi X^2 + \lambda_{SX} S^2 X^2. \quad (1)$$

where Φ denotes the SM-like doublet, while X, S are two additional real scalar fields. The model obeys an additional $\mathbb{Z}_2 \otimes \mathbb{Z}_2'$ symmetry, $\mathbb{Z}_2 : S \rightarrow -S, \mathbb{Z}_2' : X \rightarrow -X$, while all other fields transform evenly under the respective \mathbb{Z}_2 symmetry. All three scalars acquire a vacuum expectation value (vev) and therefore mix. This leads to three physical states with all possible scalar–scalar interactions.

Among the important constraints are, e.g., the Higgs signal strength measurements by the LHC experiments, perturbative unitarity as well as the requirement for the potential to be bounded from below, and current collider searches. Results have been obtained using the ScannerS [17,20,28–30] framework. Experimental results from past and current collider experiments have been implemented using the publicly available tools HiggsBounds [31–36] and HiggsSignals [37–40].

In the following, we use the convention that

$$M_1 \leq M_2 \leq M_3 \quad (2)$$

and denote the corresponding physical mass eigenstates by h_i . Gauge and mass eigenstates are related via a mixing matrix. The model contains in total nine free parameters, out of which two are fixed by the observation of a scalar particle with the mass of 125 GeV as well as electroweak precision observables. Apart from the masses, also the vacuum expectation values (vevs) and mixing angles serve as input parameters. Interactions with SM particles are then inherited from the scalar excitation of the doublet via rescaling factors κ_i , such that $g_i^{h_i AB} = \kappa_i g_i^{h_i AB, SM}$ for any $h_i AB$ coupling, where A, B denote SM particles. The orthogonality of the mixing matrix implies $\sum_i \kappa_i^2 = 1$. Furthermore, signal strength measurements require $|\kappa_{125}| \gtrsim 0.96$ [13] for the SM-like scalar h_{125} , which can be h_1, h_2 or h_3 depending on the specific parameter choice (note that the Run 2 combinations of ATLAS [1] and CMS [2] separately lead to $|\kappa_{125}| \gtrsim 0.96$ and $|\kappa_{125}| \gtrsim 0.94$, respectively. All benchmark planes in [13] fulfill these requirements).

For a certain production process (e.g., gluon gluon fusion) the cross section, σ , for h_a with mass M_a can be obtained from the corresponding SM Higgs production cross section, σ_{SM} , by simply rescaling

$$\sigma(M_a) = \kappa_a^2 \cdot \sigma_{SM}(M_a). \quad (3)$$

Since κ_a rescales all Higgs couplings to SM particles, Equation (3) is exact up to genuine electroweak corrections involving Higgs self-interactions and in particular holds to all orders in QCD.

The scaling factor κ_a plays the same role in universally rescaling the partial widths of h_a decays into SM particles, leading to

$$\Gamma(h_a \rightarrow SM; M_a) = \kappa_a^2 \cdot \Gamma_{\text{tot}}(h_{SM}; M_a), \quad (4)$$

where $\Gamma(h_a \rightarrow SM; M_a)$ denotes the sum of all partial widths of h_a into SM particle final states. In addition, the decays of branching ratios (BRs) of h_a to other scalar bosons, $h_a \rightarrow h_b h_c$, are given by

$$\text{BR}(h_a \rightarrow h_b h_c) = \frac{\Gamma_{a \rightarrow bc}}{\kappa_a^2 \Gamma_{\text{tot}}(h_{SM}) + \sum_{xy} \Gamma_{a \rightarrow xy}}. \quad (5)$$

where the denominator now denotes the total width of the scalar h_a . In the absence of BSM decay modes—which is always the case for the lightest Higgs bosons h_1 — h_a has BRs identical to a SM-like Higgs boson of the same mass.

2. Benchmark Planes

In [13], several benchmark planes (BPs) were proposed which were meant to capture mainly features that by the time of that publication were not yet addressed by searches at the LHC:

- Asymmetric production and decay, in the form of

$$pp \rightarrow h_3 \rightarrow h_1 h_2,$$

where, depending on the kinematics, $h_2 \rightarrow h_1 h_1$ decays are also possible;

- Symmetric decays in the form of

$$pp \rightarrow h_i \rightarrow h_j h_j,$$

where none of the scalars corresponds to the 125 GeV resonance. Note that this in principle allows for further decays $h_j \rightarrow h_k h_k$, again depending on the specific benchmark plane kinematics.

We list the definition of these benchmark planes in Tables 1 and 2, respectively.

Table 1. Overview of the benchmark scenarios: The second column denotes the Higgs mass eigenstate that we identify with the observed Higgs boson, h_{125} , the third column names the targeted decay mode of the resonantly produced Higgs state, and the fourth column lists possible relevant successive decays of the resulting Higgs states.

| Benchmark Scenario | h_{125} Candidate | Target Signature | Possible Successive Decays |
|--------------------|---------------------|-------------------------------|--|
| BP1 | h_3 | $h_{125} \rightarrow h_1 h_2$ | $h_2 \rightarrow h_1 h_1$ if $M_2 > 2M_1$ |
| BP2 | h_2 | $h_3 \rightarrow h_1 h_{125}$ | - |
| BP3 | h_1 | $h_3 \rightarrow h_{125} h_2$ | $h_2 \rightarrow h_{125} h_{125}$ if $M_2 > 250$ GeV |
| BP4 | h_3 | $h_2 \rightarrow h_1 h_1$ | - |
| BP5 | h_2 | $h_3 \rightarrow h_1 h_1$ | - |
| BP6 | h_1 | $h_3 \rightarrow h_2 h_2$ | $h_2 \rightarrow h_{125} h_{125}$ if $M_2 > 250$ GeV |

Table 2. Input parameter values and coupling scale factors, κ_a ($a = 1, 2, 3$), for the six defined benchmark scenarios. The doublet vev is set to $v = 246$ GeV for all scenarios.

| Parameter | Benchmark Scenario | | | | | |
|---------------|--------------------|------------|------------|----------|------------|-------------|
| | BP1 | BP2 | BP3 | BP4 | BP5 | BP6 |
| M_1 [GeV] | [1, 62] | [1, 124] | 125.09 | [1, 62] | [1, 124] | 125.09 |
| M_2 [GeV] | [1, 124] | 125.09 | [126, 500] | [1, 124] | 125.09 | [126, 500] |
| M_3 [GeV] | 125.09 | [126, 500] | [255, 650] | 125.09 | [126, 500] | [255, 1000] |
| θ_{hs} | 1.435 | 1.352 | -0.129 | -1.284 | -1.498 | 0.207 |
| θ_{hx} | -0.908 | 1.175 | 0.226 | 1.309 | 0.251 | 0.146 |
| θ_{sx} | -1.456 | -0.407 | -0.899 | -1.519 | 0.271 | 0.782 |
| v_s [GeV] | 630 | 120 | 140 | 990 | 50 | 220 |
| v_x [GeV] | 700 | 890 | 100 | 310 | 720 | 150 |
| κ_1 | 0.083 | 0.084 | 0.966 | 0.073 | 0.070 | 0.968 |
| κ_2 | 0.007 | 0.976 | 0.094 | 0.223 | -0.966 | 0.045 |
| κ_3 | -0.997 | -0.203 | 0.239 | 0.972 | -0.250 | 0.246 |

For this work, I rescanned all benchmark planes with the newest HiggsBounds and HiggsSignals versions: HiggsBounds-5.10.2 and HiggsSignals-2.6.2. For nearly all parameter points, these new versions did not introduce additional constraints on the parameter space, and I therefore show the benchmark planes from the original publication. One exception is BP5, which has a slightly more constrained parameter space taking additional searches into account. I also comment on a possible recast on this plane and give a list of current experimental searches partially relying on our model. All cross-sections that are displayed are for a center of mass (COM) energy of 13 TeV and have been derived

using rescaled predictions of the NNLO+NNLL production cross sections for an SM-like Higgs of the respective mass, as tabulated in [41]; see [13] for a more detailed discussion.

2.1. Asymmetric Decays

In this subsection, I discuss the asymmetric decay modes $h_3 \rightarrow h_1 h_2$, where successively one of the three scalars is identified with the 125 GeV resonance. I display the corresponding benchmark planes in Figure 1.

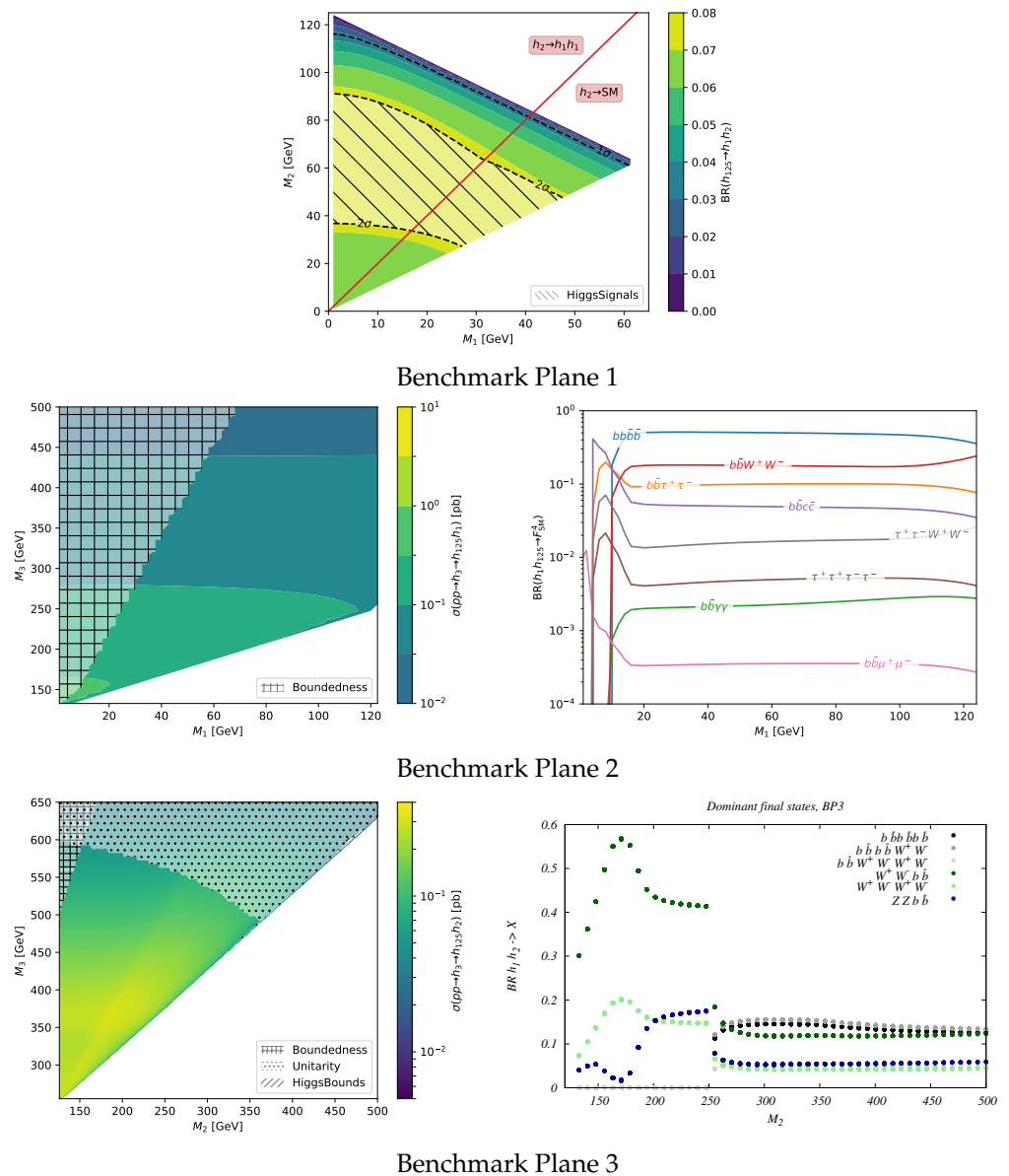


Figure 1. Benchmark planes for asymmetric production and decay, $pp \rightarrow h_3 \rightarrow h_1 h_2$, for various assignments of the 125 GeV resonance. **Top row:** BP1, where $h_3 \equiv h_{125}$. Production cross-sections are close to the SM production here, of around ~ 4 pb at 13 TeV. The branching ratio to $h_1 h_2$ is shown in the two-dimensional mass plane. **Middle and bottom rows:** BPs 2 and 3, where $h_{2,1} \equiv h_{125}$, respectively. **Left:** Production cross-sections at a 13 TeV LHC. **Right:** Branching ratios of the $h_1 h_2$ state as a function of the free light scalar mass. The slashed/hatched/dotted regions on the benchmark planes are excluded from comparison with data via HiggsBounds/HiggsSignals, the requirement that the potential must be bounded from below, and unitarity constraints. Partially taken from [13].

Depending on the benchmark plane, maximal production cross-sections are given by ~ 3 – 4 pb, ~ 0.6 pb, and 0.3 pb for $h_1 h_2$ production for BPs 1/2/3, respectively. In BP3, the

$h_1 h_1 h_1$ final state reaches cross-sections up to ~ 140 fb. Note that as soon as the kinematic threshold for $h_2 \rightarrow h_{125} h_{125}$ is reached, decays from that state in fact become dominant.

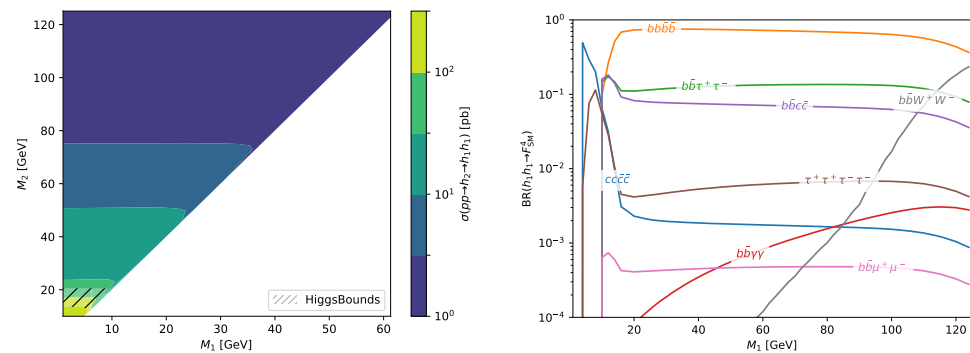
Note that the asymmetric BPs in [13] have been specifically designed such that the $h_1 h_1 h_1$ rate is enhanced as soon as the according phase space opens up. This can be in particular observed in the branching ratios for BP3 (bottom right plot in Figure 1), where, as soon as $M_2 \geq 250$ GeV, the $b\bar{b}b\bar{b}W^+W^-$ final state becomes dominant, surpassing $W^+W^-b\bar{b}$ despite the phase space and coupling suppression. This is however a particular characteristic of this particular benchmark plane.

2.2. Symmetric Decays

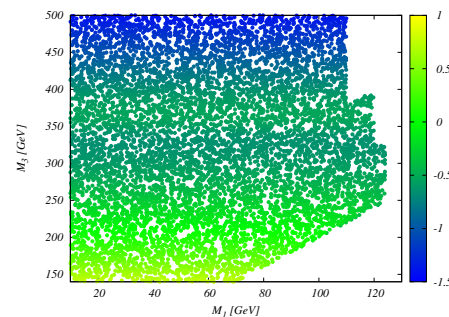
Symmetric decays are given by BPs 4/5/6, with again a differing assignment for $h_{3/2/1} \equiv h_{125}$, respectively. The corresponding production and decay modes are displayed in Figure 2.

Depending on the benchmark plane, pair-production cross-sections can reach up to 60/2.5/0.5 pb for BPs 4/5/6, respectively. For the latter, the $h_{125}h_{125}h_{125}h_{125}$ final state can reach rates up to 14 fb. In addition, note that the allowed parameter space in BP5 has slightly shrunk, mainly due to the implementation of an additional search [42] into HiggsBounds after the performance of the original scan. For BP6, six particle final states as, e.g., $W^+W^-b\bar{b}b\bar{b}$ can reach branching ratios up to $\sim 10\%$, depending on M_2 .

As before, the symmetric benchmark planes in [13] have been designed to open up interesting novel final states if the phase space allows for this; for BP6, this means that the $h_2 \rightarrow h_1 h_1$ rate has been enhanced, reaching up to 40% depending on M_2 . This again leads to the fact that branching ratios that are dominant prior to the kinematic threshold of $M_2 \sim 250$ GeV, mainly for electroweak gauge boson final states, are suppressed for larger masses. Although they remain dominant, the $W^+W^-b\bar{b}b\bar{b}$ final state displays similar rates.

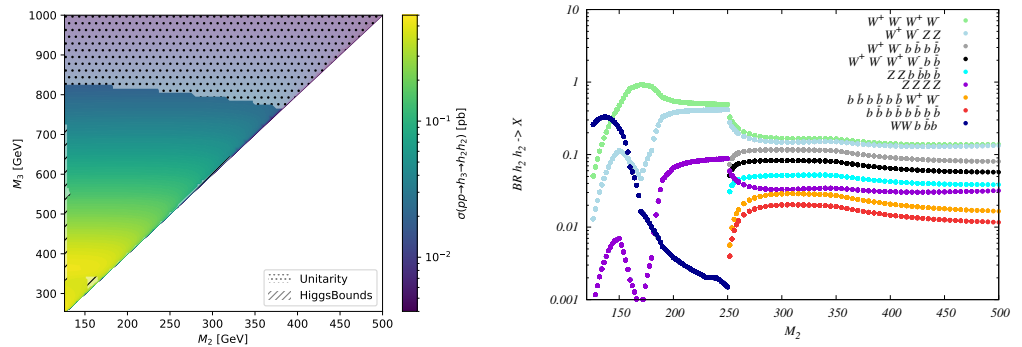


Benchmark Plane 4



Benchmark Plane 5 [color coding: $\log_{10}(\sigma_{h_3 \rightarrow h_1 h_1} / [\text{pb}])$]

Figure 2. Cont.



Benchmark Plane 6

Figure 2. Benchmark planes for symmetric production and decay, $pp \rightarrow h_i \rightarrow h_j h_j$, for various assignments of the 125 GeV resonance. **Top/middle/bottom rows:** BPs 4/5/6, where $h_{3/2/1} \equiv h_{125}$. **Left:** Production cross-sections at a 13 TeV LHC. **Right:** Branching ratios of the $h_j h_j$ state as a function of the lighter free scalar mass. Branching ratios for BP4 and 5 are identical; therefore, only one plot is displayed here. The slashed/dotted regions on the benchmark planes are excluded from comparison with data via HiggsBounds/HiggsSignals, and unitarity constraints. Partially taken from [13].

3. Further Investigation of This Model

After the original appearance of the paper proposing the TRSM, several theoretical and experimental works have been performed which at least partially build on the benchmark planes proposed here. We briefly list some of these here.

3.1. Investigation of the $h_{125}h_{125}h_{125}$ Final State

In BP3, for $M_2 \rightarrow 250$ GeV, the decay $h_2 \rightarrow h_1 h_1$ becomes dominant, leading to a $h_{125}h_{125}h_{125}$ final state. For subsequent decays into $b\bar{b}$, this BP has been investigated in [43]. We found that, depending on the parameter point and integrated luminosity, significances between 3 and ~ 10 can be achieved. I display the results in Table 3.

Table 3. The resulting selection efficiencies, $\epsilon_{\text{Sig.}}$ and $\epsilon_{\text{Bkg.}}$, number of events, S and B for the signal and background, respectively, and statistical significances. A b -tagging efficiency of 0.7 has been assumed. The numbers of signal and background events are provided at an integrated luminosity of 300 fb^{-1} . Results for 3000 fb^{-1} are obtained via simple extrapolation. The significance is given at both values of the integrated luminosity excluding (including) systematic errors in the background. Taken from [43].

| Label | (M_2, M_3) [GeV] | $\epsilon_{\text{Sig.}}$ | $S _{300\text{fb}^{-1}}$ | $\epsilon_{\text{Bkg.}}$ | $B _{300\text{fb}^{-1}}$ | $\text{sig} _{300\text{fb}^{-1}}$ (syst.) | $\text{sig} _{3000\text{fb}^{-1}}$ (syst.) |
|-------|-----------------------|--------------------------|--------------------------|--------------------------|--------------------------|--|---|
| A | (255, 504) | 0.025 | 14.12 | 8.50×10^{-4} | 19.16 | 2.92 (2.63) | 9.23 (5.07) |
| B | (263, 455) | 0.019 | 17.03 | 3.60×10^{-5} | 8.12 | 4.78 (4.50) | 15.10 (10.14) |
| C | (287, 502) | 0.030 | 20.71 | 9.13×10^{-5} | 20.60 | 4.01 (3.56) | 12.68 (6.67) |
| D | (290, 454) | 0.044 | 37.32 | 1.96×10^{-4} | 44.19 | 5.02 (4.03) | 15.86 (6.25) |
| E | (320, 503) | 0.051 | 31.74 | 2.73×10^{-4} | 61.55 | 3.76 (2.87) | 11.88 (4.18) |
| F | (264, 504) | 0.028 | 18.18 | 9.13×10^{-5} | 20.60 | 3.56 (3.18) | 11.27 (5.98) |
| G | (280, 455) | 0.044 | 38.70 | 1.96×10^{-4} | 44.19 | 5.18 (4.16) | 16.39 (6.45) |
| H | (300, 475) | 0.054 | 41.27 | 2.95×10^{-4} | 66.46 | 4.64 (3.47) | 14.68 (4.94) |
| I | (310, 500) | 0.063 | 41.43 | 3.97×10^{-4} | 89.59 | 4.09 (2.88) | 12.94 (3.87) |
| J | (280, 500) | 0.029 | 20.67 | 9.14×10^{-5} | 20.60 | 4.00 (3.56) | 12.65 (6.66) |

Note that we also compared how different channels, e.g., direct decays of the heavier scalars into VV or $h_{125}h_{125}$ final states, would perform at an HL-LHC. The results are displayed in Figure 3.

We note that all benchmark points that were investigated can additionally be probed by other production and decay mechanisms. Note, however, that these test different regions

of the parameter space, as they depend on different parameters in the potential. These searches can therefore be considered to be complementary.

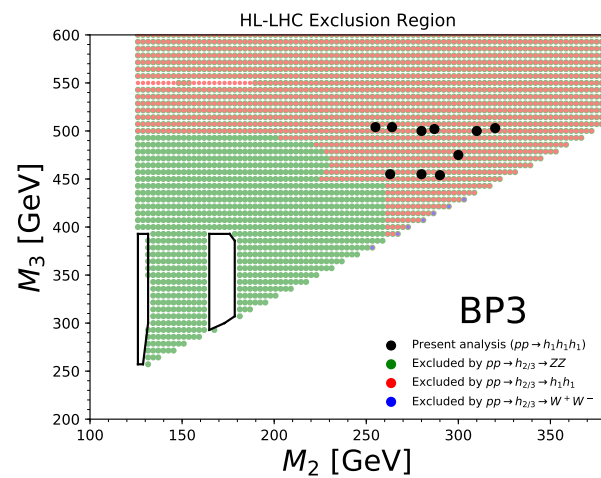


Figure 3. The expected exclusion region for the full integrated luminosity of the HL-LHC, 3000 fb^{-1} , through final states *other* than $pp \rightarrow h_1 h_1 h_1$ as explained in the main text. Points with green circles are expected to be excluded by ZZ final states, with red circles by $h_1 h_1$ and with blue circles by $W^+ W^-$. The $W^+ W^-$ analysis excludes only very few points on the parameter space and therefore appears infrequently in the figure. The points **A–I** that we have considered in our analysis of $pp \rightarrow h_1 h_1 h_1$ are shown in black circles overlaid on top of the circles indicating the exclusion. The two cut-out white regions near $M_2 \sim 130 \text{ GeV}$ and $M_2 \sim 170 \text{ GeV}$ will remain viable at the end of the HL-LHC. Taken from [43].

3.2. Recasting Current LHC Searches

It is also interesting to investigate whether current searches can be reinterpreted and recasted in such a way that they allow us to exclude regions in the models' parameter space that were not directly scrutinized in the experimental search, or for which no interpretation was presented in the original publication. In [44], the authors have reinterpreted a CMS search for $pp \rightarrow H \rightarrow h_{125} h_{125} \rightarrow 4b$ [45], which corresponds to di-Higgs production via a heavy resonance and subsequent decays into $b\bar{b}$ final states, and extended the mass ranges for the scalars in the decay chain. I have applied these results to the TRSM, in particular to BP5. I display the corresponding results in Figure 4 (I thank the authors of [44] for providing us with the corresponding exclusion limits). We see that the sensitive region of parameter space is significantly extended, and therefore, an actual experimental analysis also in this parameter region is greatly encouraged.

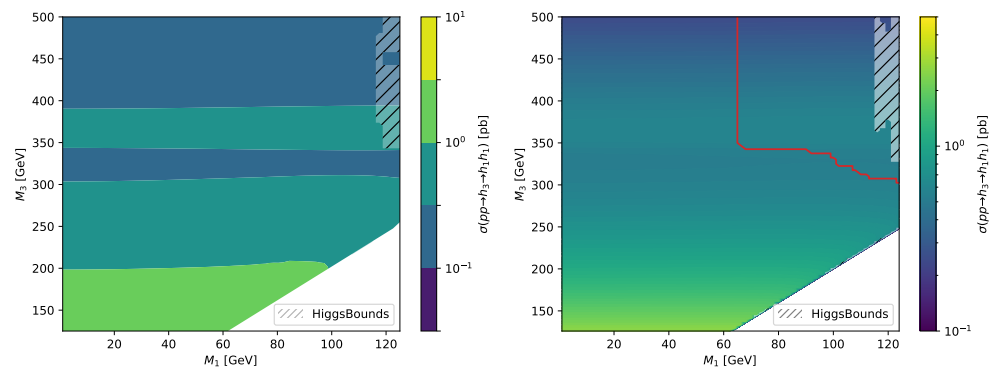


Figure 4. Reinterpretation of a 36 fb^{-1} CMS search for di-Higgs production via a heavy resonance using the $4b$ final state. The exclusion line uses the results obtained in [44]. Points to the right and above the red contour are excluded. The slashed regions on the benchmark planes are excluded from comparison with data via HiggsBounds/HiggsSignals. Taken from [46].

3.3. Experimental Searches with TRSM Interpretations

Two experimental searches have by now made use of the predictions obtained within the TRSM to interpret regions in parameter space that are excluded: a CMS search for asymmetric production and subsequent decay into $b\bar{b}b\bar{b}$ final states [11], as well as $b\bar{b}\gamma\gamma$ in [12]. For this, maximal production cross sections were provided in the parameter space, allowing all additional new physics parameter to float; the respective values have been tabulated in [47,48]. Figures 5 and 6 show the expected and observed limits in these searches for the TRSM and NMSSM [49].

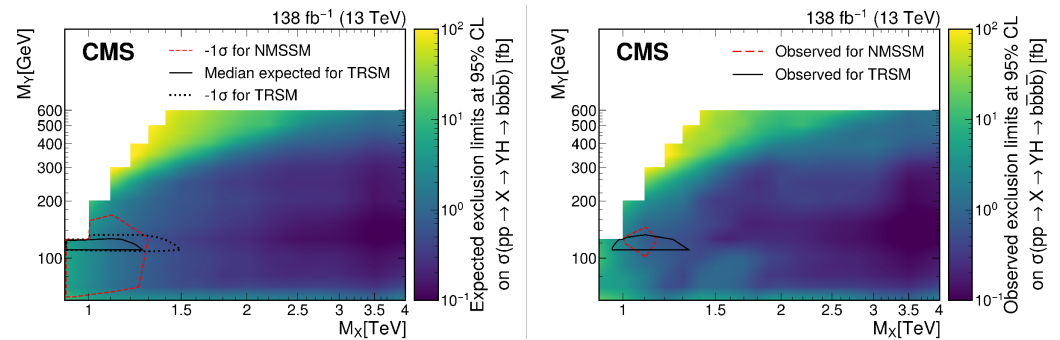


Figure 5. Expected (left) and observed (right) 95% confidence limits for the $pp \rightarrow h_3 \rightarrow h_2 h_1$ search, with subsequent decays into $b\bar{b}b\bar{b}$. For both models, maximal mass regions up to $m_3 \sim 1.4$ TeV, $m_2 \sim 140$ GeV can be excluded. Figure taken from [11].

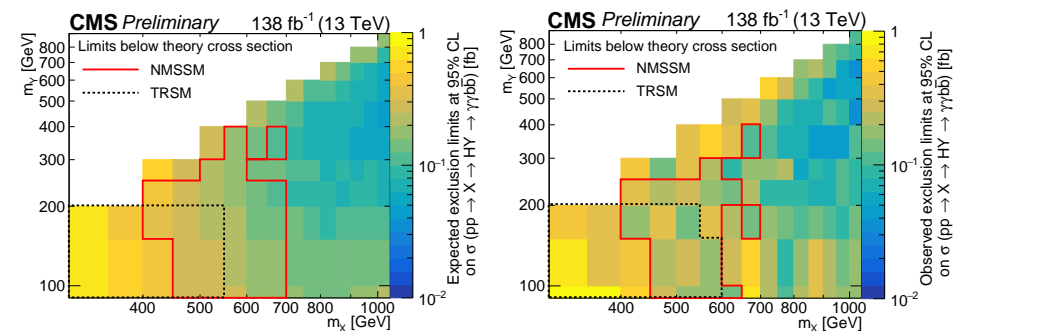


Figure 6. Expected (left) and observed (right) 95% confidence limits for the $pp \rightarrow h_3 \rightarrow h_2 h_1$ search, with subsequent decays into $b\bar{b}\gamma\gamma$. Depending on the model, maximal mass regions up to $m_3 \sim 800$ GeV, $m_2 \sim 400$ GeV can be excluded. Figure taken from [12].

In addition, several searches also investigate decay chains that can in principle also be realized within the TRSM, as, e.g., other searches for the same final states [50] or $b\bar{b}\mu^+\mu^-$ [51] final states.

4. Signatures at Higgs Factories

The investigation of light scalars has recently gained again more interest after the recommendation of the European Strategy Report [52,53] to concentrate on e^+e^- machines with $\sqrt{s} \sim 240\text{--}250$ GeV. A short review about the current state of the art for such searches and models that allow for low scalars can, e.g., be found in [8]. In this model, the only feasible production is Zh radiation of the lighter scalar, with production cross-sections given in Figure 7. Cross-sections have been derived using Madgraph5 [54].

We can now investigate what would be production cross-sections for scalar particles with masses $\lesssim 160$ GeV at Higgs factories.

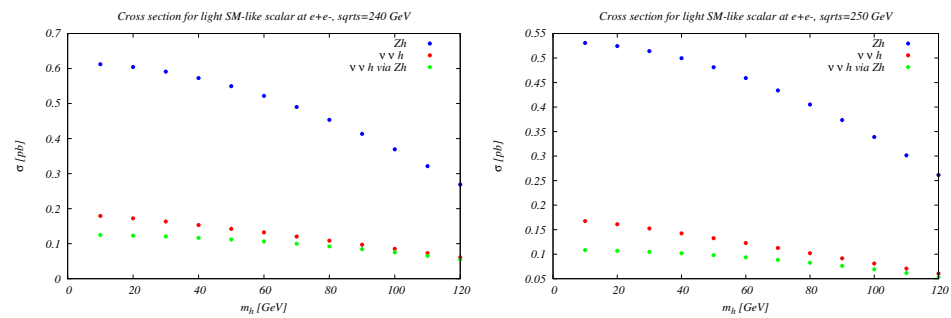


Figure 7. Leading order production cross-sections for Zh and $h\nu_\ell\bar{\nu}_\ell$ production at an e^+e^- collider with a COM energy of 240 GeV (left) and 250 GeV (right) using Madgraph5 for an SM-like scalar h . The contribution of Zh to $\nu_\ell\bar{\nu}_\ell h$ using a factorized approach for the Z decay is also shown. Taken from [8].

4.1. Production of 125 GeV Resonance and Subsequent Decays

We first turn to the easy case of the production of the 125 GeV resonance in various benchmark scenarios. Of interest are cases where decays $h_{125} \rightarrow h_i h_j$ are kinematically allowed. Note that our benchmark points were not set up in particular for the scenario where $i = j$, and so rates might be relatively small by construction.

From Table 2, we see that for all scenarios, the rescaling for the 125 GeV resonance is $\gtrsim 0.966$, leading to production cross-sections of about ~ 0.2 pb, close to the SM value. In general, due to constraints from the invisible branching ratio [55] as well as signal strength fits, the production cross-section for $h_i h_j$ final states has to be lower by at least an order of magnitude, leading to cross-sections $\mathcal{O}(10$ fb). In fact, in the benchmark planes presented here, the largest rate for $Z h_{125}$ production and subsequent scalar decays can be found in BP1, where the rates are given by multiplying the BRs from Figure 1 with the production of $Z h_{125}$, giving maximal cross-sections of around 18 fb.

4.2. Additional Scalar Production

We now turn to the Higgs-Strahlung production of new physics scalars. This process is in principle possible for all BPs discussed here. However, if we require production rates of $Z h_i$ to be larger than ~ 10 fb, only BPs 4 and 5 render sufficiently large rates for the production of h_2 and h_3 , respectively. Production rates are independent of the other scalars, and we therefore depict them for both BPs in Figure 8. Note that BP4 and BP5 have slightly different parameter settings; in particular, the absolute value of $\kappa_3 = -0.250$ in BP5 is slightly larger than the absolute value of $\kappa_2 = 0.223$ in BP4, leading to a discontinuity for the production cross section predictions in that figure.

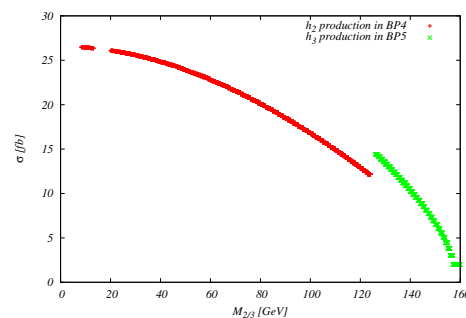


Figure 8. Production cross-sections for $Zh_{2/3}$ in BPs 4 and 5, respectively, at a 250 GeV Higgs factory.

BP4 is constructed in such a way that as soon as the corresponding parameter space opens up, the $h_1 h_1$ decay becomes dominant; final states are therefore mainly $Z b\bar{b}b\bar{b}$ if $M_2 \gtrsim 2 M_1$. Below that threshold, dominant decays are into a $b\bar{b}$ pair, which means that standard searches as, e.g., presented in [56,57] should be able to cover the parameter space.

Similarly, in BP5, the $h_3 \rightarrow h_1 h_1$ decay is also favored as soon as it is kinematically allowed. Therefore, in this parameter space, again $Zb\bar{b}\bar{b}$ final states become dominant. Otherwise, $Zb\bar{b}$ and ZW^+W^- final states prevail, with a cross-over for the respective final states at around $M_3 \sim 135$ GeV. Branching ratios for these final states are in the 40–50% regime.

5. More General Scan

So far, I have constrained myself to the discussion of the benchmark planes that were presented in [13]. However, of course, it is also of interest to consider generic scans of the model, and/or other parameter regions. An example for this has already been given above, where a more generic parameter region was investigated in [11,47].

Here, I plan to concentrate on scenarios that are accessible at future Higgs factories. One reason for this is that while the BPs in [13] were especially designed to focus on by that time non-explored signatures at the LHC, the production and decay processes at lepton colliders are slightly more constrained, as stated above. Second, the inclusion of additional low-mass scalars might help to reduce the discrepancy between the SM prediction and experimental PDG value of the W-boson mass; see, e.g., an early discussion in [58] in the context of a real singlet extension.

I start by presenting the general result of a scan in the 2 mass or 1 mass 1 mixing angle plane already given in [8,59], given in Figure 9. In this figure, two data-sets are considered that fulfill all current constraints, as implemented using the current versions of ScannerS and HiggsBounds, HiggsSignals. The are labelled “low–low” if both $M_{1,2} \leq 125$ GeV and “high–low” if $M_1 \leq 125$ GeV, $M_3 \geq 125$ GeV.

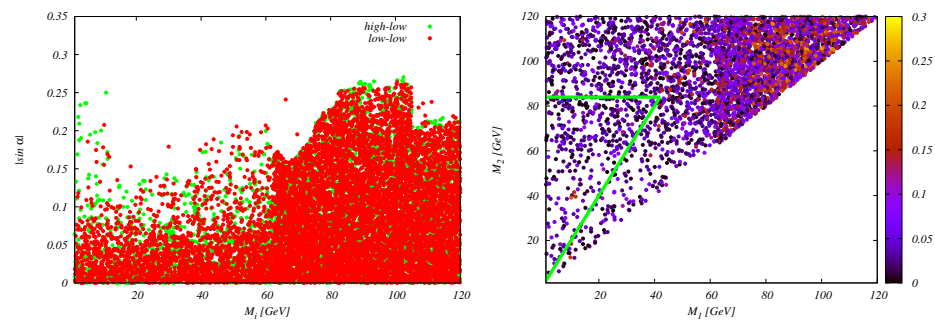


Figure 9. Available parameter space in the TRSM, with one (high–low) or two (low–low) masses lighter than 125 GeV. **Left:** light scalar mass and mixing angle, with $\sin \alpha = 0$ corresponding to complete decoupling. **Right:** available parameter space in the (M_1, M_2) plane, with color coding denoting the rescaling parameter $\sin \alpha$ for the lighter scalar h_1 . Within the green triangle, $h_{125} \rightarrow h_2 h_1 \rightarrow h_1 h_1 h_1$ decays are kinematically allowed. Taken from [8].

In that plot, $|\sin \alpha|$ is symbolic for the respective mixing angle, earlier denoted by κ_i , where $\sin \alpha = 0$ would correspond to the complete decoupling. We see that, in general, for low mass scalars, mixing angles up to ~ 0.3 are still allowed. This also in principle can lead to slightly higher production rates than discussed in the previous section.

5.1. W-Boson Mass in the TRSM

In general, for extensions of the scalar sector by one or several gauge-singlets, the contributions to the W-boson mass can be factorized into a SM and a new physics part, as discussed in [58] for a real singlet extension. The extension of this for an additional singlet is straightforward, leading to the following expression of $\Delta(\delta\rho_{\text{TRSM}})$:

$$\Delta(\delta\rho_{\text{TRSM}}) = \sum_i \Delta(\delta\rho_{\text{sing}})(M_i; \kappa_i)$$

where $\Delta(\delta\rho_{\text{sing}})(M_i; \sin\alpha_i)$ is given by Equation (26) of [58] with the replacement $m_{H^0} \rightarrow M_i$, $\sin\alpha \rightarrow \kappa_i$, and $M_i \neq 125$ GeV in the above sum. The relation $\sum_i \kappa_i^2 = 1$ ensures in fact that the above relation holds in general for a model with an arbitrary number of singlet extensions.

In the comparison with the current measurement of the W-boson mass [60],

$$M_W^{\text{exp}} = (80.377 \pm 0.012) \text{ GeV},$$

We have also updated the input values for the SM prediction, as already presented in [7], i.e., we use

$$\begin{aligned} \alpha_s(M_Z) &= 0.1179; & M_h &= 125.25 \text{ GeV}; & M_t &= 172.76 \text{ GeV}; \\ M_Z &= 91.1876; & \Delta\alpha_{\text{had}} &= 276 \times 10^{-4}; & \Delta\alpha_{\text{lep}} &= 314.979 \times 10^{-4}, \end{aligned}$$

which gives $M_W^{\text{SM}} = 80.356$ GeV as the SM prediction, following the calculation outlined in [61].

We then evaluate the new physics contributions to the W-boson mass by extending the code presented in [58] by contributions from a second scalar, where the mass is determined recursively as discussed in that work, and compare it to the current experimental value given above, requiring an at most 2σ discrepancy. As expected, for the “low–low” dataset introduced above where $M_3 \equiv M_{125}$, corrections drive the W-boson mass prediction closer to the SM, so none of the points is excluded by requiring a maximal 2σ discrepancy. On the other hand, for the “high–low” dataset, where $M_2 \equiv M_{125}$, points with masses and mixing angles $m_3 \gtrsim 200$ GeV, $|\kappa_3| \gtrsim 0.15$ can be ruled out; cf. Figure 10, where the maximally allowed mixing angle is mass-dependent.

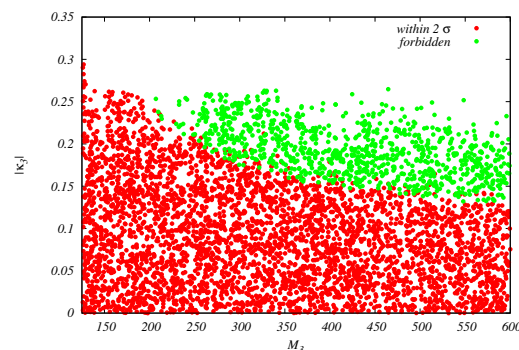


Figure 10. Allowed (red) and excluded (green) regions in the $(M_3; |\kappa_3|)$ plane for the “high–low” dataset, where $M_3 \gtrsim M_{125}$. Regions roughly above $M_3 \gtrsim 200$ GeV, $|\kappa_3| \gtrsim 0.15$ can be excluded requiring a maximal 2σ discrepancy between prediction and experimentally allowed value.

Finally, one can ask whether the current $\sim 1.8\sigma$ discrepancy between experimental value and SM prediction can be significantly reduced within the TRSM taking new physics contributions into account. In general, this would require relatively light masses, together with large mixing angles for such masses. In the datasets investigated here, the maximal value for the W-boson mass was around $M_W \sim 80.361$ GeV. This is in fact a point in the high–low dataset, where however the heavier scalar is nearly decoupled. The exact input parameters for this point are given by

$$M_1 = 4.2 \text{ GeV}, M_3 = 494 \text{ GeV}, \kappa_1 = 0.24, \kappa_3 = 0.016.$$

In general, scenarios with lightest scalars with masses $M_1 \lesssim 12$ GeV, $|\kappa_1| \gtrsim 0.15$ give the largest positive corrections to the W-boson mass. Several of such points exist in both the high–low and low–low datasets, cf. Figure 9 (left). The above discussion also shows that, taking into account all current constraints, the TRSM cannot explain even larger deviations

for the W-boson mass, as, e.g., the values reported in [62] that range from 80.433 ± 9 GeV to 80.424 ± 9 GeV for single measurement and combination, respectively.

5.2. Production Cross Sections at a Higgs Factory

Finally, we investigate the maximal allowed production cross-section at Higgs factories, where, as before, we chose $\sqrt{s} = 250$ GeV as a benchmark center-of-mass energy. As discussed above, Zh production is dominant in the low mass range and also makes the largest contribution to the $\nu\bar{\nu}h$ final state, so we concentrate on Higgs-strahlung.

We show maximally allowed production cross-sections at an e^+e^- collider with a COM energy of 250 GeV in Figure 11. Note that we do not display the region where $M_i \sim 125$ GeV; here, when the other scalars are close to being decoupled (in the sense that $|\kappa_i| \sim 0$), we recover production cross-sections around 250 fb, as predicted for the SM using the LO approach discussed here.

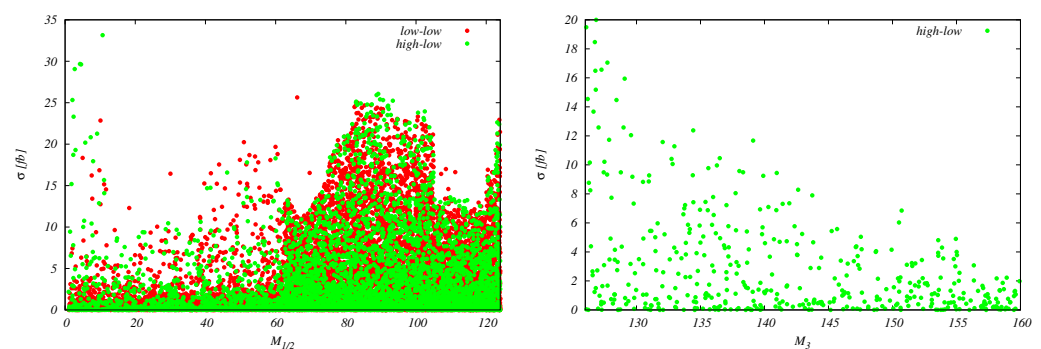


Figure 11. Maximal production cross-section for Higgs-strahlung for scalars of masses $\neq 125$ GeV in the TRSM for points passing all discussed constraints. Production cross-sections depend on the parameter point and can reach up to 30 fb.

As branching ratios for the low mass scalars are inherited via mixing with the scalar from the SM-like doublet, the largest production cross-sections are obtained for scenarios where the light scalars decay into $b\bar{b}$ final states. For such final states, several studies already exist projecting bounds at Higgs factories; see, e.g., discussion and references in [8]. We display cross-sections for such final states in Figure 12, together with predictions for $h_1 h_1$ final states in case $h_2 \rightarrow h_1 h_1$. In the mass range $M_i \lesssim 12$ GeV, $\tau\tau$ and $c\bar{c}$ final states can additionally lead to cross sections up to 20 fb.

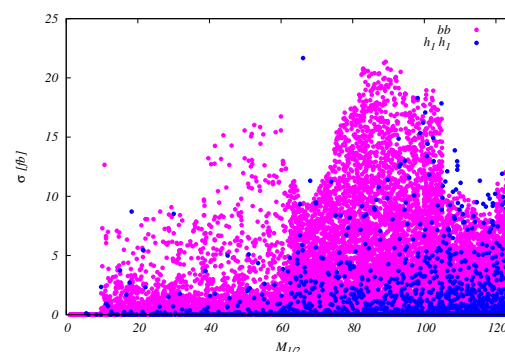


Figure 12. Production cross sections for $e^+e^- \rightarrow Zh_{1/2} \rightarrow ZX X$, with $X \equiv b$ (magenta) and h_1 (blue). Points from all data sets are included. Cross sections can reach up to 20 fb. In the low mass region, also $X \equiv \tau, c$ final states can become important (not shown here).

For the region $M_3 \gtrsim 126$ GeV, three different decay channels are dominant: $h_1 h_1$, $W^+ W^-$, and $b\bar{b}$. We display the corresponding production cross-sections in Figure 13.

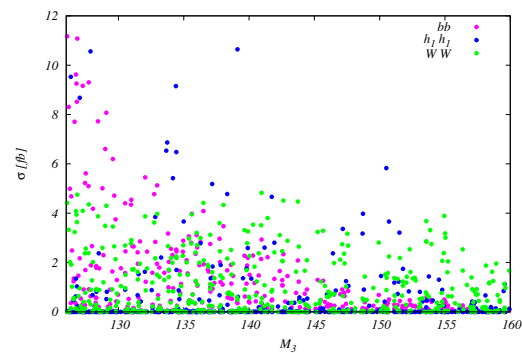


Figure 13. Production cross-sections for $e^+e^- \rightarrow Zh_3 \rightarrow ZXX$, with $X \equiv b$ (magenta), h_1 (blue), and W (green). Points from all data sets are included. Cross-sections can reach up to ~ 12 fb.

Finally, we can ask what cross-sections can be obtained for $e^+e^- \rightarrow Zh_{2/3}$, with subsequent decays to h_1h_1 final states. Again, ignoring cases where $M_i \sim 125$ GeV, we display the corresponding cross-sections in Figure 14. We find the largest cross-section of about ~ 20 fb for a parameter point where $M_2 \sim 66$ GeV, $M_1 \sim 18$ GeV. The h_1 in this parameter point decays predominantly into $b\bar{b}$ final states with a branching ratio of about 85%.

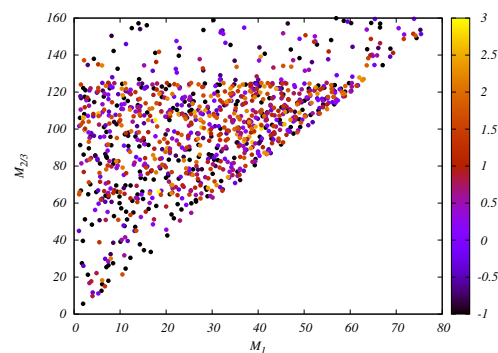


Figure 14. Production cross-sections for $e^+e^- \rightarrow Zh_{2/3} \rightarrow ZXX$, with $X \equiv h_1$, in the $(M_1, M_{2/3})$ plane. Color coding refers to the $\log_{10}[\sigma/\text{fb}]$ for Zh_1h_1 production. Maximal cross-sections are around 20 fb.

6. Summary

In this manuscript, I gave a short summary of the status of collider signatures and searches in the TRSM introduced in [13]. I gave a summary of the current state of the art and investigation, including further detailed collider studies, recasts, as well as current searches that use or are motivated by this model. I also gave a brief overview on channels within this model that might be testable at future e^+e^- machines, with a focus on Higgs factories with $\sqrt{s} \sim 250$ GeV. Finally, I commented on regions that would be allowed or excluded by the current value of the W-boson mass.

Funding: This research received no external funding.

Data Availability Statement: Data points for figures can be made available upon request.

Conflicts of Interest: The author declares no conflict of interest.

References

1. The ATLAS Collaboration. A detailed map of Higgs boson interactions by the ATLAS experiment ten years after the discovery. *Nature* **2022**, *607*, 52–59. [[CrossRef](#)] [[PubMed](#)]
2. A portrait of the Higgs boson by the CMS experiment ten years after the discovery. *Nature* **2022**, *607*, 60–68. [[CrossRef](#)] [[PubMed](#)]

3. Pruna, G.M.; Robens, T. Higgs singlet extension parameter space in the light of the LHC discovery. *Phys. Rev. D* **2013**, *88*, 115012. [[CrossRef](#)]
4. Robens, T.; Stefaniak, T. Status of the Higgs Singlet Extension of the Standard Model after LHC Run 1. *Eur. Phys. J. C* **2015**, *75*, 104. [[CrossRef](#)]
5. Robens, T.; Stefaniak, T. LHC Benchmark Scenarios for the Real Higgs Singlet Extension of the Standard Model. *Eur. Phys. J. C* **2016**, *76*, 268. [[CrossRef](#)]
6. Robens, T. More Doublets and Singlets. In Proceedings of the 56th Rencontres de Moriond on Electroweak Interactions and Unified Theories, La Thuile, Italy, 12–19 March 2022.
7. Papaefstathiou, A.; Robens, T.; White, G. Signal strength and W-boson mass measurements as a probe of the electro-weak phase transition at colliders—Snowmass White Paper. In Proceedings of the 2022 Snowmass Summer Study, Seattle, WA, USA, 17–26 July 2022.
8. Robens, T. A Short Overview on Low Mass Scalars at Future Lepton Colliders. *Universe* **2022**, *8*, 286. [[CrossRef](#)]
9. Lewis, I.M.; Sullivan, M. Benchmarks for Double Higgs Production in the Singlet Extended Standard Model at the LHC. *Phys. Rev. D* **2017**, *96*, 035037. [[CrossRef](#)]
10. Chen, C.Y.; Kozaczuk, J.; Lewis, I.M. Non-resonant Collider Signatures of a Singlet-Driven Electroweak Phase Transition. *J. High Energy Phys.* **2017**, *2017*, 96. [[CrossRef](#)]
11. CMS Collaboration. Search for a massive scalar resonance decaying to a light scalar and a Higgs boson in the four b quarks final state with boosted topology. *arXiv* **2022**, arXiv:2204.12413.
12. CMS Collaboration. Search for a New Resonance Decaying to Two Scalars in the Final State with Two Bottom Quarks and Two Photons in Proton-Proton Collisions at $\sqrt{s} = 13$ TeV; Technical Report; CERN: Geneva, Switzerland, 2022.
13. Robens, T.; Stefaniak, T.; Wittbrodt, J. Two-real-scalar-singlet extension of the SM: LHC phenomenology and benchmark scenarios. *Eur. Phys. J. C* **2020**, *80*, 151. [[CrossRef](#)]
14. Robens, T. TRSM Benchmark Planes—Snowmass White Paper. In Proceedings of the 2022 Snowmass Summer Study, Seattle, WA, USA, 17–26 July 2022.
15. Barger, V.; Langacker, P.; McCaskey, M.; Ramsey-Musolf, M.; Shaughnessy, G. Complex Singlet Extension of the Standard Model. *Phys. Rev.* **2009**, *D79*, 015018. [[CrossRef](#)]
16. Alexander-Nunneley, L.; Pilaftsis, A. The Minimal Scale Invariant Extension of the Standard Model. *J. High Energy Phys.* **2010**, *2010*, 21. [[CrossRef](#)]
17. Coimbra, R.; Sampaio, M.O.P.; Santos, R. ScannerS: Constraining the phase diagram of a complex scalar singlet at the LHC. *Eur. Phys. J.* **2013**, *C73*, 2428. [[CrossRef](#)]
18. Ahriche, A.; Arhrib, A.; Nasri, S. Higgs Phenomenology in the Two-Singlet Model. *J. High Energy Phys.* **2014**, *2014*, 42. [[CrossRef](#)]
19. Costa, R.; Morais, A.P.; Sampaio, M.O.P.; Santos, R. Two-loop stability of a complex singlet extended Standard Model. *Phys. Rev.* **2015**, *D92*, 025024. [[CrossRef](#)]
20. Costa, R.; Mühlleitner, M.; Sampaio, M.O.P.; Santos, R. Singlet Extensions of the Standard Model at LHC Run 2: Benchmarks and Comparison with the NMSSM. *J. High Energy Phys.* **2016**, *2016*, 34. [[CrossRef](#)]
21. Ferreira, P.M. The vacuum structure of the Higgs complex singlet-doublet model. *Phys. Rev.* **2016**, *D94*, 096011. [[CrossRef](#)]
22. Chang, J.; Cheung, K.; Hsu, S.C.; Lu, C.T. Detecting multimuon jets from the Higgs boson exotic decays in the Higgs portal framework. *Phys. Rev.* **2017**, *D95*, 035012. [[CrossRef](#)]
23. Mühlleitner, M.; Sampaio, M.O.P.; Santos, R.; Wittbrodt, J. Phenomenological Comparison of Models with Extended Higgs Sectors. *J. High Energy Phys.* **2017**, *2017*, 132. [[CrossRef](#)]
24. Dawson, S.; Sullivan, M. Enhanced di-Higgs boson production in the complex Higgs singlet model. *Phys. Rev.* **2018**, *D97*, 015022. [[CrossRef](#)]
25. aali, J.O.; Manaut, B.; Rahili, L.; Semlali, S. Naturalness implications within the two-real-scalar-singlet beyond the SM. *Eur. Phys. J. C* **2021**, *81*, 1045. [[CrossRef](#)]
26. Ghosh, S. Oblique parameters of BSM models with three CP-even neutral scalars. *arXiv* **2022**, arXiv:2201.01006.
27. Adhikari, S.; Lane, S.D.; Lewis, I.M.; Sullivan, M. Complex Scalar Singlet Model Benchmarks for Snowmass. In Proceedings of the 2022 Snowmass Summer Study, Seattle, WA, USA, 17–26 July 2022.
28. Ferreira, P.M.; Guedes, R.; Sampaio, M.O.P.; Santos, R. Wrong sign and symmetric limits and non-decoupling in 2HDMs. *J. High Energy Phys.* **2014**, *2014*, 67. [[CrossRef](#)]
29. Mühlleitner, M.; Sampaio, M.O.P.; Santos, R.; Wittbrodt, J. The N2HDM under Theoretical and Experimental Scrutiny. *J. High Energy Phys.* **2017**, *2017*, 94. [[CrossRef](#)]
30. Mühlleitner, M.; Sampaio, M.O.P.; Santos, R.; Wittbrodt, J. ScannerS: Parameter scans in extended scalar sectors. *Eur. Phys. J. C* **2022**, *82*, 198. [[CrossRef](#)]
31. Bechtle, P.; Brein, O.; Heinemeyer, S.; Weiglein, G.; Williams, K.E. HiggsBounds: Confronting Arbitrary Higgs Sectors with Exclusion Bounds from LEP and the Tevatron. *Comput. Phys. Commun.* **2010**, *181*, 138–167. [[CrossRef](#)]
32. Bechtle, P.; Brein, O.; Heinemeyer, S.; Weiglein, G.; Williams, K.E. HiggsBounds 2.0.0: Confronting Neutral and Charged Higgs Sector Predictions with Exclusion Bounds from LEP and the Tevatron. *Comput. Phys. Commun.* **2011**, *182*, 2605–2631. [[CrossRef](#)]

33. Bechtle, P.; Brein, O.; Heinemeyer, S.; Stal, O.; Stefaniak, T.; Weiglein, G.; Williams, K. Recent Developments in HiggsBounds and a Preview of HiggsSignals. *PoS* **2012**, *CHARGED2012*, 24. [[CrossRef](#)]
34. Bechtle, P.; Brein, O.; Heinemeyer, S.; Stål, O.; Stefaniak, T.; Weiglein, G.; Williams, K.E. HiggsBounds—4: Improved Tests of Extended Higgs Sectors against Exclusion Bounds from LEP, the Tevatron and the LHC. *Eur. Phys. J. C* **2014**, *74*, 2693. [[CrossRef](#)]
35. Bechtle, P.; Heinemeyer, S.; Stal, O.; Stefaniak, T.; Weiglein, G. Applying Exclusion Likelihoods from LHC Searches to Extended Higgs Sectors. *Eur. Phys. J. C* **2015**, *75*, 421. [[CrossRef](#)]
36. Bechtle, P.; Dercks, D.; Heinemeyer, S.; Klingl, T.; Stefaniak, T.; Weiglein, G.; Wittbrodt, J. HiggsBounds-5: Testing Higgs Sectors in the LHC 13 TeV Era. *Eur. Phys. J. C* **2020**, *80*, 1211. [[CrossRef](#)]
37. Stål, O.; Stefaniak, T. Constraining extended Higgs sectors with HiggsSignals. *PoS* **2013**, *EPS-HEP2013*, 314. [[CrossRef](#)]
38. Bechtle, P.; Heinemeyer, S.; Stål, O.; Stefaniak, T.; Weiglein, G. *HiggsSignals*: Confronting arbitrary Higgs sectors with measurements at the Tevatron and the LHC. *Eur. Phys. J. C* **2014**, *74*, 2711. [[CrossRef](#)]
39. Bechtle, P.; Heinemeyer, S.; Stål, O.; Stefaniak, T.; Weiglein, G. Probing the Standard Model with Higgs signal rates from the Tevatron, the LHC and a future ILC. *J. High Energy Phys.* **2014**, *11*, 039. [[CrossRef](#)]
40. Bechtle, P.; Heinemeyer, S.; Klingl, T.; Stefaniak, T.; Weiglein, G.; Wittbrodt, J. HiggsSignals-2: Probing new physics with precision Higgs measurements in the LHC 13 TeV era. *Eur. Phys. J. C* **2021**, *81*, 145. [[CrossRef](#)]
41. Andersen, J.R.; Artoisenet, P.; Bagnaschi, E.A.; Banfi, A.; Becher, T.; Bernlochner, F.U.; Bolognesi, S.; Bolzoni, P.; Boughezal, R.; Buarque, D.; et al. *Handbook of LHC Higgs Cross Sections: 3. Higgs Properties*; CERN: Geneva, Switzerland, 2013. [[CrossRef](#)]
42. Aaboud, M.; Aad, G.; Abbott, B.; Abdinov, O.; Abeloos, B.; Abidi, S.H.; AbouZeid, O.S.; Abraham, N.L.; Abramowicz, H.; Abreu, H.; et al. Search for pair production of Higgs bosons in the $b\bar{b}b\bar{b}$ final state using proton-proton collisions at $\sqrt{s} = 13$ TeV with the ATLAS detector. *J. High Energy Phys.* **2019**, *2019*, 30. [[CrossRef](#)]
43. Papaefstathiou, A.; Robens, T.; Tetlalmatzi-Xolocotzi, G. Triple Higgs Boson Production at the Large Hadron Collider with Two Real Singlet Scalars. *J. High Energy Phys.* **2021**, *2021*, 193. [[CrossRef](#)]
44. Barducci, D.; Mimasu, K.; No, J.M.; Vernieri, C.; Zurita, J. Enlarging the scope of resonant di-Higgs searches: Hunting for Higgs-to-Higgs cascades in $4b$ final states at the LHC and future colliders. *J. High Energy Phys.* **2020**, *2020*, 2. [[CrossRef](#)]
45. Sirunyan, A.M.; et al. Search for resonant pair production of Higgs bosons decaying to bottom quark-antiquark pairs in proton-proton collisions at 13 TeV. *J. High Energy Phys.* **2018**, *2018*, 152. [[CrossRef](#)]
46. Robens, T. Models with (broken) Z_2 symmetries. *PoS* **2022**, *DISCRETE2020-2021*, 63. [[CrossRef](#)]
47. Robens, T. $b\bar{b}b\bar{b}$ Final States in the TRSM for Asymmetric Production and Decay. Available online: <https://twiki.cern.ch/twiki/pub/LHCPhysics/LHCHWG3EX/rep.pdf> (accessed on 2 December 2021).
48. Robens, T. trsm_bbaga.txt. Available online: <https://twiki.cern.ch/twiki/bin/view/LHCPhysics/LHCHWG3EX> (accessed on 27 September 2022).
49. Ellwanger, U.; Hugonie, C. Benchmark planes for Higgs-to-Higgs decays in the NMSSM. *Eur. Phys. J. C* **2022**, *82*, 406. [[CrossRef](#)]
50. Tumasyan, A.; Adam, W.; Andrejkovic, J.W.; Bergauer, T.; Chatterjee, S.; Damanakis, K.; Dragicevic, M.; Escalante Del Valle, A.; Frühwirth, R.; Jeitler, M.; et al. Search for new particles in an extended Higgs sector with four b quarks in the final state at $s=13$ TeV. *Phys. Lett. B* **2022**, *835*, 137566. [[CrossRef](#)]
51. Aad, G.; Abbott, B.; Abbott, D.C.; Abed Abud, A.; Abeling, K.; Abhayasinghe, D.K.; Abidi, S.H.; Aboulhorma, A.; Abramowicz, H.; Abreu, H.; et al. Search for Higgs boson decays into a pair of pseudoscalar particles in the $b\bar{b}\mu\mu$ final state with the ATLAS detector in pp collisions at $\sqrt{s}=13$ TeV. *Phys. Rev. D* **2022**, *105*, 012006. [[CrossRef](#)]
52. Abramowicz, H.; Forty, R. *Physics Briefing Book: Input for the European Strategy for Particle Physics Update 2020*; Fermi National Accelerator Lab. (FNAL): Batavia, IL, USA, 2019.
53. Group, E.S. *2020 Update of the European Strategy for Particle Physics*; Technical Report; CERN Council: Geneva, Switzerland, 2020. [[CrossRef](#)]
54. Alwall, J.; Herquet, M.; Maltoni, F.; Mattelaer, O.; Stelzer, T. MadGraph 5: Going Beyond. *J. High Energy Phys.* **2011**, *2011*, 128. [[CrossRef](#)]
55. *Combination of Searches for Invisible Higgs Boson Decays with the ATLAS Experiment*. Technical Report; CERN: Geneva, Switzerland, 2020. Available online: <https://atlas.web.cern.ch/Atlas/GROUPS/PHYSICS/CONFNOTES/ATLAS-CONF-2020-052> (accessed on 22 October 2020).
56. Drechsel, P.; Moortgat-Pick, G.; Weiglein, G. Prospects for direct searches for light Higgs bosons at the ILC with 250 GeV. *Eur. Phys. J. C* **2020**, *80*, 922. [[CrossRef](#)]
57. Wang, Y.; Berggren, M.; List, J. ILD Benchmark: Search for Extra Scalars Produced in Association with a Z boson at $\sqrt{s} = 500$ GeV. *arXiv* **2020**, arXiv:2005.06265.
58. López-Val, D.; Robens, T. Δr and the W-boson mass in the singlet extension of the standard model. *Phys. Rev. D* **2014**, *90*, 114018. [[CrossRef](#)]
59. Robens, T. A short overview on low mass scalars at future lepton colliders—Snowmass White Paper. In Proceedings of the 2022 Snowmass Summer Study, Seattle, WA, USA, 17–26 July 2022.
60. Particle Data Group; Workman, R.L.; Burkert, V.D.; Crede, V.; Klempt, E.; Thoma, U.; Tiator, L.; Agashe, K.; Aielli, G.; Allanach, B.C.; et al. Review of Particle Physics. *Prog. Theor. Exp. Phys.* **2022**, *2022*, 083C01.

61. Awramik, M.; Czakon, M.; Freitas, A.; Weiglein, G. Precise prediction for the W boson mass in the standard model. *Phys. Rev. D* **2004**, *69*, 053006. [[CrossRef](#)]
62. Aaltonen, T.; Amerio, S.; Amidei, D.; Anastasov, A.; Annovi, A.; Antos, J.; Apollinari, G.; Appel, J.A.; Arisawa, T.; Artikov, A.; et al. High-precision measurement of the W boson mass with the CDF II detector. *Science* **2022**, *376*, 170–176. [[CrossRef](#)]

Disclaimer/Publisher’s Note: The statements, opinions and data contained in all publications are solely those of the individual author(s) and contributor(s) and not of MDPI and/or the editor(s). MDPI and/or the editor(s) disclaim responsibility for any injury to people or property resulting from any ideas, methods, instructions or products referred to in the content.